## Motion Control of an Autonomous Wheel-Leg Bikebot

Xinyan Huang, Feng Han, Yi Han, Shuoyu Wang, Tao Liu, and Jingang Yi

Abstract—An autonomous bikebot (i.e., bicycle-like robot) is an attractive single-track platform for off-road, agile navigation applications. It is challenging for bikebots to navigate at low velocity on off-road, cluttered terrains. In this paper, we design a wheel-leg hybrid bikebot control system. The bikebot control can switch between different actuation modes. At low-speed movement and on off-road, bumpy terrains, the regular steering-induced balance torque itself cannot effectively balance the platform and the leg-assisted balance torque is used. A model predictive control is designed for the leg assistive actuation to take advantage of the leg-ground interaction force and balance torque. By doing so, the bikebot can safely navigate and balance in various off-road environments. High-fidelity simulation results are presented to demonstrate that the wheelleg bikebot can efficiently navigate at low speed in cluttered space and keep balance on bumpy terrains.

#### I. Introduction

Autonomous bikebot (i.e., bicycle-like mobile robot) is a type of single-track, underactuated, wheel-based robots [1]. Under the speed and steering control, bikebot can follow a given trajectory and meanwhile maintain the platform balance [2], [3]. Many research work focus on bikebot navigation and balancing control design theoretically and experimentally with relatively high speed [4]-[8]. One of the major challenges for bikebot control is that the steeringinduced balance torque is limited and a large steering angle does not always generate a significant balance torque [8]-[10]. At low speed or stationary, it is almost impossible to balance the bikebot only by using steering input [11]. To improve balance capability, various balance assistive devices have been designed, including the inverted pendulum, reaction wheels, and gyro-balancers, etc. [12], [13]. It is desirable to build a robust, reliable platform and control system for bikebot to safely navigate on off-road, bumpy terrains.

Comparing with wheeled robots, legged robots such as bipedal robots have demonstrated the great potentials for applications on off-road or rocky terrains [14]–[16]. The benefits of the legged robots' ability for off-road, challenging

This work was supported in part by the National Science Foundation of China (NSFC) under awards 52175033 and U21A20120 (Liu) and US National Science Foundation (NSF) under award CNS-1932370 (Yi).

terrains or cluttered environments come at the price of complicated structure and high degree of freedom (DOFs). Furthermore, the moving velocity of legged robots is usually much smaller than wheel robots. To take the advantages of both wheel and legged robots, we design a wheel-leg hybrid bikebot for off-road and bumpy terrain applications. Unlike most of the reported wheel-leg robots (e.g., [17]), the wheels and legs are arranged in a parallel, rather than cascade, fashion. This wheel-leg parallel structure enables an easy switch between the wheel- or leg-mode cooperation. The wheel-leg bikebot can travel on different terrain conditions, i.e., flat surface or narrow and rugged terrains. In the wheellocomotion mode, the navigation is based on the steering and velocity control, while in the leg-locomotion mode, control actuation comes from the leg-ground interaction force together with steering and velocity regulations.

The challenges in controlling the wheel-leg bikebot include the leg-ground interaction actuation design and the coordination of the controlled leg-steering motion. The legground interaction control requires high frequency implementation (e.g., 500 Hz) and switches between position and force control modes due to precise force and torque regulation requirement. The bikebot steering and velocity control is implemented at a relative low frequency (e.g., 50-100 Hz). When designing the leg-ground interaction forces, both the balance torque and forward-thrusting force need to be considered simultaneously. We build a hybrid dynamics model for the bikebot that is easily switched and adapted to different control modes. The wheel mode control is in an external and internal convertible (EIC) form and the planar motion and balance motion stability is guaranteed simultaneously [4]. A model predictive control (MPC) is proposed to design the leg-ground interaction force when the bikebot navigates in cluttered environment with limited velocity. We further coordinate the leg actuation and steering control to improve the tracking performance and improve balance robustness on off-road, rugged terrains. The contribution of the paper mainly lies in the wheel-leg bikebot design and the coordinated steering-leg control strategy for various terrain conditions. The wheel-leg hybrid bikebot has different control modes, taking the advantages of the regular wheel and leg robots, and therefore, can adapt to different terrain conditions and expand to various applications. Comparing with the previous work in [11] in which the leg impulse is used as additional assistive balance actuation at high-speed movement crossing the obstacles, the leg actuation in this work is continuously applied to the bikebot under low-speed movement.

The remainder of the paper is outlined as follows. Sec-

X. Huang and T. Liu are with the State Key Lab of Fluid Power and Mechatronic Systems and the School of Mechanical Engineering, Zhejiang University, Hangzhou, Zhejiang 310027 China (email: hxinyan@zju.edu.cn; liutao@zju.edu.cn).

Y. Han and S. Wang are with the Department of Intelligent Mechanical Systems Engineering, Kochi University of Technology 185 Miyanokuchi, Tosayamada-cho, Kami-city 782-8502, Japan (e-mail: 258012g@gs.kochi-tech.ac.jp; wang.shuoyu@kochi-tech.ac.jp).

F. Han and J. Yi are with the Department of Mechanical and Aerospace Engineering, Rutgers University, Piscataway, NJ 08854 USA (e-mail: fh233@scarletmail.rutgers.edu; jgyi@rutgers.edu).

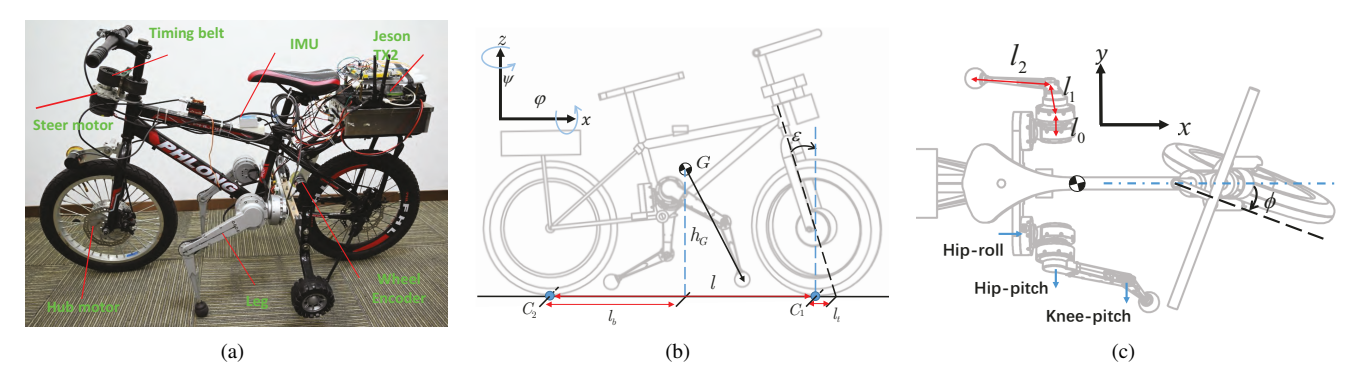


Fig. 1. (a) Prototype of the wheel-leg bikebot with two assistive legs. (b) Side view and (c) top view of the wheel-leg bikebot schematic.

tion II discusses the design of the wheel-leg bikebot system and its dynamics model. In Section III, we present the motion control design of the wheel-leg bikebot. The simulation results are presented in Section IV. Finally, Section V summarizes the concluding remarks.

# II. WHEEL-LEG BIKEBOT DESIGN AND DYNAMICS MODEL

#### A. System Design

Fig. 1(a) shows the prototype of the wheel-leg bikebot. The bikebot is modified from a front wheel driven bicycle with various sensors and actuators. Unlike most of the wheel-leg robots, two 3-DOF auxiliary legs are mounted symmetrically to the lower part of the bikebot frame. The wheel and the two legs are arranged in a parallel structure and this enables the coordination between the wheel and leg locomotion simultaneously.

In order to meet the need of high-performance computation, the onboard embedded system includes a lowerlevel real-time microcontroller (STM32F4) and a upperlevel computer (NVIDIA Jetson TX2). The upper computer communicates with the lower microcontroller through the UART serial port, and then drives the hub and steer motor indirectly. The leg motors are operated by the upper-level computer through a controller area network (CAN) bus at a frequency of 500 Hz. Two encoders are used to measure bikebot steering angle and the wheel velocity. An inertial measurement unit (IMU) is used for obtaining bikebot attitude and acceleration. Table I lists the main systems components and specifications. Fig. 2 further illustrates the integration schematic of the onboard embedded systems with the sensors and actuators. To improve the real-time performance and computation need, the control algorithm was implemented in C++ and deployed in Ubuntu operating system with a real-time kernel. The multi-threaded task scheduling scheme was used in control system implementation. Various task framework with running frequencies and priorities are shown in Fig. 2.

### B. System Dynamics Model

The motion of the bikebot considered in this work includes the planar motion and roll motion. Fig. 1(b) illustrates the

TABLE I COMPONENTS OF THE BIKEBOT PROTOTYPE

Component	Name	Manufacturer		
Hub Motor	LF-12	Li Feng Motor		
Steer Motor	QDD LITE-PR60-36	INNFOS		
Assistive Leg	Yobotics Leg	Yobotics		
Motor Battery	ACE LiPo 3300mAh 10S	Grepow		
Computer Battery	ACE LiPo 4000mAh 3S	Grepow		
Leg Battery	ACE LiPo 4000mAh 4S	Grepow		
Microcontroller	STM32F429	ST		
Onboard Computer	Jetson Tx2	NVIDIA		
IMU	WTGAHRS2	WitMotion		
Wheel Encoder	E6B2-CWZ3E	OMRON		

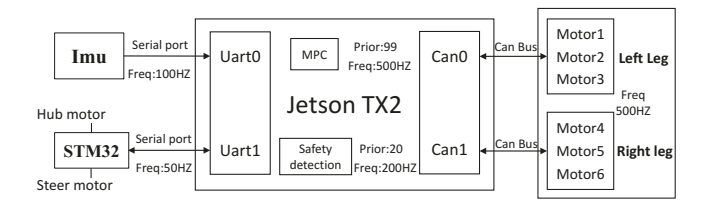


Fig. 2. Schematic of the embedded system integration with sensors and actuators for the wheel-leg bikebot.

bikebot kinematic configuration. We denote the front and rear wheel-ground contact points as  $C_1$  and  $C_2$ , respectively. We choose the rear wheel ground contact point  $C_2$  to represent the planar motion of the bikebot and its position is denoted as  $\mathbf{r} = [x \ y]^T$  in the inertia frame that is fixed on the ground with the Z-axis pointing upward. The horizontal moving frame is defined as the z-axis pointing upwards and the xaxis aligning with  $C_1C_2$ ; see Fig. 1(b). The bikebot's roll angle, yaw angle and steering angle are denoted as  $\varphi, \psi, \phi$ , respectively as shown in Figs. 1(b) and 1(c). The mass of the robot is denoted as m, and G denotes the center of mass (COM). The moment of inertia of the wheel-leg bikebot around the x-axis is denoted as  $J_b$ . The horizontal and vertical distances from the COM to  $C_2$  are denoted as  $l_b$  and  $h_G$ , respectively. The length of  $C_1C_2$  is denoted as l, the caster angle is denoted as  $\varepsilon$ , and the front wheel trail is denoted as  $l_t$ . The forward speed of the rear wheels is considered as v.

The legs are considered as two 3-DOF robotic arms with the hip, thigh, and calf joints. The joint angles and link lengths are denoted as  $\theta_0$ ,  $\theta_1$ ,  $\theta_2$ , and  $l_0$ ,  $l_1$ ,  $l_2$ , respectively. The nonholonomic constraint at  $C_2$  gives  $\dot{x}=v\,c_\psi$ ,  $\dot{y}=v\,s_\psi$ , where for convenience of expression we take notation convention  $s_\psi=\sin\psi$  and  $c_\psi=\cos\psi$  for angle  $\psi$  and other angles throughout the paper. Taking the third order derivative of r, we obtain

$$\boldsymbol{r}^{(3)} = \begin{bmatrix} x^{(3)} \\ y^{(3)} \end{bmatrix} = -\underbrace{\begin{bmatrix} v\dot{\psi}\,c_{\psi} + 2\dot{v}\,s_{\psi} \\ v\dot{\psi}\,s_{\psi} - 2\dot{v}\,c_{\psi} \end{bmatrix}}_{\boldsymbol{F}_{\psi}} \dot{\psi} + \underbrace{\begin{bmatrix} c_{\psi} & -v\,s_{\psi} \\ s_{\psi} & v\,c_{\psi} \end{bmatrix}}_{\boldsymbol{G}_{\psi}} \boldsymbol{u},$$

where  $\boldsymbol{u} = [u_v \ u_\psi]^T$ ,  $u_v = \ddot{v}$ , and  $u_\psi = \ddot{\psi}$ . From [18], the yaw angular rate is calculated as  $\dot{\psi} = \frac{v \ c_\varphi}{l \ c_\varphi} \tan \phi$  and  $u_\psi$  is

$$u_{\psi} = \frac{\dot{v} \tan \phi c_{\varepsilon}}{l c_{\varphi}} + \frac{v c_{\varepsilon}}{l c_{\varphi}} (\sec^{2}_{\phi} \dot{\phi} + \tan \phi \tan \varphi \dot{\varphi}). \quad (2)$$

The Lagrangian of the roll motion of the system is

$$L = \frac{1}{2}J_b\dot{\varphi}^2 + \frac{1}{2}m\mathbf{v}_G^T \cdot \mathbf{v}_G - mg(h_G \,\mathrm{c}_\varphi - \Delta h_G), \quad (3)$$

where  $v_G = [v_r + h\dot{\psi}s_{\varphi}\ (l_b\dot{\psi} - h\dot{\varphi}c_{\varphi})\ - h\dot{\varphi}s_{\varphi}]^T$  denotes the velocity of the COM, and  $\Delta h_G = \frac{l_b l_t \tan \phi_g \, c_\varepsilon}{l} \, s_{\varphi}$  is to account for the COM height change due to steering effect, and  $\phi_g = \arctan\left(\frac{\tan \phi \, c_\varepsilon}{c_{\varphi}}\right)$  is the projected steering angle. Using the Lagrange method, the dynamics of the bikebot roll motion is obtained as

$$J_t \ddot{\varphi} = f(\varphi) + g(\varphi)u_{\psi},\tag{4}$$

where  $J_t = mh_G^2 + J_b$ ,  $g(\varphi) = mh_G l_b c_{\varphi}$ ,  $f(\varphi) = mh_G v_r \dot{\psi} c_{\varphi} + mh_G^2 \dot{\psi}^2 s_{\varphi} c_{\varphi} + mgh_G s_{\varphi} + \frac{mgl_b l_t \tan \phi_g c_{\varepsilon}}{l} c_{\varphi}$ .

When the leg interacts with the ground, balance torque is also generated. Let  ${}^{yz}f_i=[f_{iy}\ f_{iz}]^T$  denote the ground reaction force of the *i*th leg in the yz direction, i=1,2 for the left and right legs, respectively. The ground reaction torque induced by  ${}^{yz}f_i$  is given by

$$\boldsymbol{\tau}_{ia} = {}^{yz}\boldsymbol{r}_i \times {}^{yz}\boldsymbol{f}_i, \tag{5}$$

where  ${}^{yz}r_i=[r_{i_y}\,r_{i_z}]^T$  is the displacement of the ith leg relative to the  $C_1C_2$  axis. For instance,  $r_y$  and  $r_z$  for the left leg are

$$\begin{split} r_y &= c_{\varphi}(l_y + l_0 \, c_{\theta_0} - l_1 \, s_{\theta_0} \, c_{\theta_1} - l_2 \, s_{\theta_0} \, c_{\theta_1 + \theta_2}) \\ &- s_{\varphi}(h_b + l_0 \, s_{\theta_0} + l_1 \, c_{\theta_0} \, c_{\theta_1} + l_2 \, c_{\theta_0} \, c_{\theta_1 + \theta_2}), \quad \text{(6a)} \\ r_z &= - s_{\varphi}(l_y + l_0 \, c_{\theta_0} - l_1 \, s_{\theta_0} \, c_{\theta_1} - l_2 \, s_{\theta_0} \, c_{\theta_1 + \theta_2}) \\ &- c_{\varphi}(h_b + l_0 \, s_{\theta_0} + l_1 \, c_{\theta_0} \, c_{\theta_1} + l_2 \, c_{\theta_0} \, c_{\theta_1 + \theta_2}) \quad \text{(6b)} \end{split}$$

where  $l_y$  denotes the distance from the fist joint to  $C_1C_2$ . The balance torque is the component of  $\tau_{ig}$  in the x direction.

We assume that the torque in the x direction (pitch) is encountered by the gravity of the robot itself and the displacement of the wheel in the y direction (lateral) is neglected. The longitudinal force  $f_{ix}$  still generates the thrust

for the robot forward motion and therefore,  $\dot{v} = \frac{f_{ix}}{m}$ . The entire system model is finally written as

$$\mathbf{r}^{(3)} = -\mathbf{F}_{\psi}\dot{\psi} + \mathbf{G}_{\psi}\mathbf{u} + \mathbf{G}_{\psi}\begin{bmatrix} \frac{\dot{f}_{ix}}{m} \\ 0 \end{bmatrix}$$
(7a)

$$J_t \ddot{\varphi} = f(\varphi) + g(\varphi)u_{\psi} + \tau_{iq_x}, \tag{7b}$$

where  $\tau_{ig_x}$  denotes the balance torque from leg-ground interaction. In the next section, we design the bikebot control under the steering and leg-ground interaction force actuation.

#### III. MOTION CONTROL DESIGN

In this section, we first present the EIC control for the bikebot control. We then design the leg-ground interaction force and balance torque through an MPC method.

#### A. Steering Control Design

Without considering the leg-ground interaction, for a given trajectory  $\mathbf{r}_d = [x_d \ y_d]^T$ , the tracking control is designed based on (1) as

$$\boldsymbol{u} = \boldsymbol{G}_{\psi}^{-1} (\boldsymbol{F}_{\psi} \dot{\psi} + \boldsymbol{u}_r), \tag{8}$$

where  $u_r = r_d^{(3)} + a_2 \ddot{e}_r + a_1 \dot{e}_r + a_0 e_r$  is the auxiliary control input, the tracking error  $e_r = r - r_d$ , and  $a_i > 0$ , i = 0, 1, 2, are properly selected feedback gains. Under the control (8), the trajectory tracking error  $e_r$  converges to zero asymptotically. However the balance requirement is not fulfilled yet. To incorporate the balance task, the roll motion is enforced to move along the balance equilibrium manifold (BEM) [18] under  $u = [u_v \ u_\psi]^T$  in (8) as

$$\mathcal{E} = \{ \varphi^e : f(\varphi^e) + g(\varphi^e) u_\psi = 0 \}. \tag{9}$$

Using the BEM as the desired profile of the roll motion, the balance control is updated as

$$\bar{u}_{ab} = q^{-1}(\varphi) \left[ J_t u_b - f(\varphi) \right], \ u_b = \ddot{\varphi}^e + b_1 \dot{e}_b + b_0 e_b, \ (10)$$

where  $b_0, b_1 > 0$  and  $e_b = \varphi - \varphi^e$ . The final control design incorporates both the above trajectory tracking and balance control, that is,

$$\bar{\boldsymbol{u}} = [u_v \ \bar{u}_w]^T. \tag{11}$$

Under (11), the closed-loop system errors for both the trajectory tracking and roll balance converge to a small ball around zero exponentially [4].

#### B. Leg Actuation Design

When moving on rugged terrain, the bikebot cannot maintain a high speed for safety concern. For low-speed motion, instead of relying only on the steering balance effect, we consider to use the leg-ground interaction force to fulfill the trajectory tracking and balance task.

The model (7) with leg actuation then is simplified as

$$\dot{x} = v c_{\psi}, \ \dot{y} = v s_{\psi}, \ \dot{\psi} = \frac{v c_{\varepsilon}}{l c_{\omega}} \tan \phi, \ \dot{v} = \frac{f_{ix}}{m},$$
 (12a)

$$J_t \ddot{\varphi} = mgh_G \,\mathbf{s}_{\varphi} + \tau_{iq_x} + f_1(\varphi) + g(\varphi)u_{\psi},\tag{12b}$$

where  $f_1(\varphi) = f(\varphi) - mgh_G s_{\varphi}$  and  $u_{\psi}$  is the steering control. At low speed, the steering balance effect  $g(\varphi)u_{\psi}$  is not significant. Instead we use the leg-ground interaction torque to balance the bikebot. To design the leg-ground interaction force, let  $\chi = [\varphi \ v \ \dot{\varphi} \ \dot{v}]^T$  and we obtain that

$$\dot{\chi} = A\chi + BF + D,\tag{13}$$

where

$$m{A} = egin{bmatrix} 0 & 0 & 1 & 0 \ 0 & 0 & 0 & 1 \ rac{mgh_G}{J_t} & 0 & 0 & 0 \ 0 & 0 & 0 & 0 \ \end{pmatrix}, m{F} = egin{bmatrix} m{f_1} \ m{f_2} \end{bmatrix},$$

 $f_i = [f_{i_x} \ f_{i_y} \ f_{i_z}]^T, \ i=1,2$ , is the leg-ground interaction force,  $D = [0\ 0\ 0\ f_1(\varphi) + g(\varphi)u_\psi]^T$  and  $B = [P_1\ P_2]$  with

$$m{P}_i = egin{bmatrix} 0 & 0 & 0 \ 0 & 0 & 0 \ 0 & rac{-r_{z_i}}{J_t} & rac{r_{y_i}}{J_t} \ rac{1}{m} & 0 & 0 \end{pmatrix}, \ i = 1, 2.$$

We need to design the leg locomotion gait and legground interaction forces to control balancing of the bikebot. For (13), we formulate the following MPC problem to design the leg-ground interaction force

$$\min_{\mathcal{F}} \int_{t}^{t+H\delta_{t}} \left( e^{T} Q e + F^{T} W F \right) d\tau$$
 (14a)

Subj. to: 
$$\dot{\chi} = A\chi + BF + D$$
,  $t \le \tau \le t + H\delta_t$ , (14b)

$$\underline{c}_i \le (CF)_i \le \overline{c}_i, j = 1, \cdots, 5,$$
 (14c)

where  $\mathcal{F} = \{ \boldsymbol{F}(t), \dots, \boldsymbol{F}(t+H\delta_t) \}$  is the control set for  $\tau \in [t,t+H\delta_t]$ ,  $\delta_t$  is the time step length,  $H \in \mathbb{N}$  is the predictive horizon,  $\boldsymbol{e} = \chi - \chi^d, \chi_d$  is the desired velocity and roll angle,  $\boldsymbol{Q}$  and  $\boldsymbol{W}$  are diagonal weight matrices. Matrix  $\boldsymbol{C}$  is

$$m{C} = egin{bmatrix} m{C}_1 & m{C}_2 \end{bmatrix}, m{C}_i = egin{bmatrix} -1 & 1 & 0 & 0 & 0 \ 0 & 0 & -1 & 1 & 0 \ \mu & \mu & \mu & \mu & 1 \end{bmatrix}^T,$$

 $\mu$  is the leg-ground contact friction coefficient,  $\underline{c}, \overline{c} \in \mathbb{R}^6$  represent the lower- and upper-limits of the friction and motor torque physical constraints, respectively, and subscript j in (14c) represents the jth element of the vector. We further discretize and solve (14) in real time by using the qpOASES algorithm [19].

The leg-ground interaction force input acts on the bikebot like a sequence of balance torques. When the ith leg touches down on the ground, the joint torque to generate the expected ground reaction force  $f_i$  is computed by

$$\boldsymbol{\tau}_i = \boldsymbol{J}_i^T \boldsymbol{R}_i^T \boldsymbol{f}_i \tag{15}$$

where R is the rotation transformation matrix from the body frame to the inertia frames, and  $J \in \mathbb{R}^{3\times3}$  is the

Jacobian matrix of the foot contact point that is obtained by differentiating the foot position vector.

The leg gait is obtained by designing the expected foot position. When the bikebot moves forward, the swing leg foot position  $p^{\text{des}}$  is designed using the following heuristic function inspired by [20]

$$\boldsymbol{p}^{\mathrm{des}} = \boldsymbol{p}^{\mathrm{hip}} + \frac{\boldsymbol{v}_G T_s}{2} + k_p (\boldsymbol{v} - \boldsymbol{v}^{\mathrm{ref}}),$$

where  $T_s$  is the gait cycle duration,  $\boldsymbol{p}^{\mathrm{hip}}$  is the position of hip in the xy plane,  $\boldsymbol{v}^{\mathrm{ref}} = [v_x \, v_y]^T$  is the nominal velocity of the bikebot,  $\boldsymbol{v}_G$  is the COM velocity, and  $k_p$  is the gain.

#### IV. SIMULATION RESULTS

In this section, we use simulation to demonstrate the motion controller of the wheel-leg bikebot. The simulation is based on the prototype that is described in Section II-A.

We created various scenarios to test the proposed control algorithm design. We conducted the test in a high-fidelity simulation environment that is provided by the RaiSim package [21]. The RaiSim simulation uses a physics engine and therefore is capable to conduct realistic simulation studies. A physical model of the wheel-leg hybrid bikebot was created from the CAD design directly. The designed embedded control system scheme as shown in Fig. 2 was used and implemented in simulation. Fig. 3 shows the created simulation scenario in RaiSim as one illustrative example with three steps.

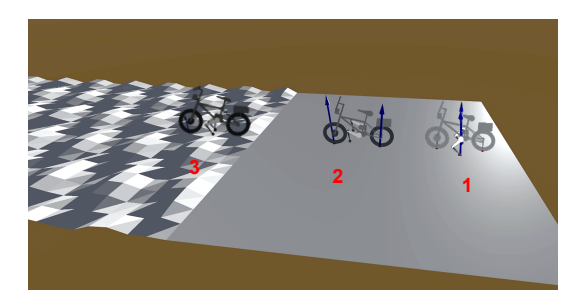


Fig. 3. Illustration of the simulation environment in RaiSim.

Table II lists the values of the physical model parameters of the bikebot. The wheel-leg bikebot steering control was implemented at 50 Hz and the leg control was conducted at 500 Hz. The other control design parameters are  $\boldsymbol{W} = \text{diag}(1e-5,1e-5,1e-5,1e-5,1e-5)$ ,  $\boldsymbol{Q} = \text{diag}(10,1,1,1)$ ,  $\mu = 0.45$ , H = 4,  $\delta T = 0.06$  s,  $T_s = 0.15$  s,  $a_1 = 3$ ,  $a_2 = 6$ ,  $a_3 = 10$ ,  $b_1 = 180$ , and  $b_2 = 25$ .

We first demonstrate the leg actuation control result. Assuming that the bikebot is at the space with multiple objects surrounded, the control target is to move from a starting to an ending points to follow a desired trajectory. Due to environment constraint, leg actuation was used to create thrust force to generate forwarding motion and create balance torque at the same time. Fig. 4 shows the simulation results. Fig. 4(a) shows the bikebot trajectory along with the assistive leg foot contact points on the ground. The bikebot moved from the origin to follow a given desired trajectory. Fig. 4(b) shows the bikebot velocity. The velocity was maintained at

TABLE II  $Physical\ parameters\ of\ the\ bikebot\ and\ the\ legs$ 

ĺ	m <sub>b</sub> (kg)	$J_b \text{ (kgm}^2)$	$J_t \text{ (kgm}^2)$	l (m)	$R_w$ (m)	$l_t/h_G$ (m)	$l_b/l$ (m)	$\varepsilon$ (deg)	$l_j$ (m)	$l_x, l_y$ (m)	$\tau_{\theta_j}^{\mathrm{max}}$ (Nm)	$\theta_j^{\rm max}/\theta_j^{\rm min}$ (deg)
	25	0.8	4.13	0.87	0.21	0.064/0.365	0.42/0.87	17	0.075/0.212/0.220	0.1/0.13	24	150/-150

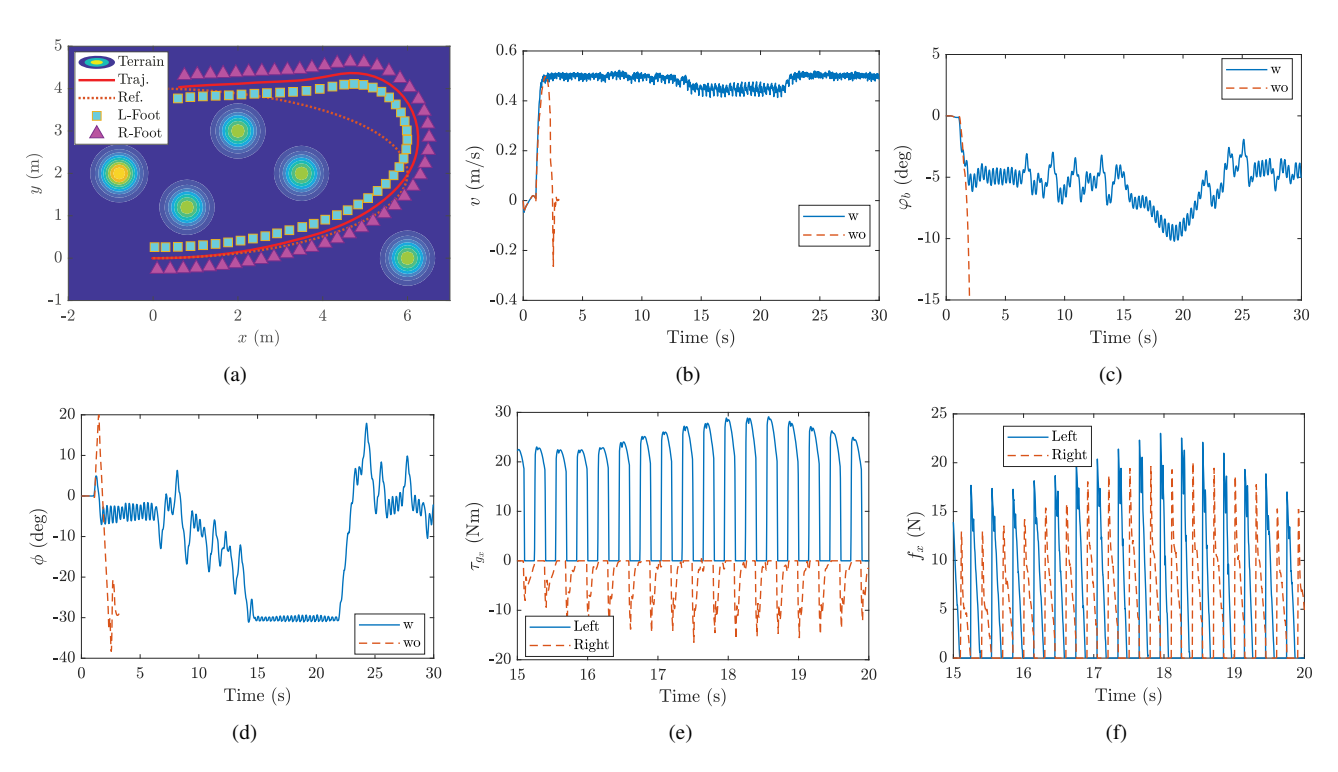


Fig. 4. Low-speed bikebot motion control in a narrow space. (a) Bikebot trajectory with the leg footprint. (b) Bikebot velocity v. (c) Bikebot roll angle  $\varphi_b$ . (d) Steering angle  $\phi$ . (e) Leg-ground balance torque  $\tau_{g_x}$ . (f) Leg-ground interaction force  $f_x$ . The legends "w" and "wo" in (b) to (d) indicate the cases with and without using leg actuation, respectively.

0.5 m/s, which is small compared with the regular bicycle riding speed. Fig. 4(c) shows the bikebot roll angle and it demonstrated a small vibration around 5 deg. Notice that at t = 15 s, the bikebot needed to make a turn and the steering angle reached the maximum allowed value around 30 deg as shown in Fig. 4(d) and this caused large tracking errors as shown in Fig. 4(a). The steering-induced torque for a large steering angle also became large, indicating a requirement of leg actuation for additional balance torque. Figs. 4(e) and 4(f) show the leg-ground balance torque  $\tau_{q_x}$  and force  $f_x$ , respectively. The left and right legs repeatedly touched on the ground to generate the force and balance torque. The balance torque reached 25 Nm, which is much larger than the steering-induced balance torque at v = 0.5 m/s. The spikes in Figs. 4(e) and 4(f) are due to the foot touchdown detection and leg control switch. For comparison, we include the steering-only control results in Fig. 4(c) and it is clear that the bikebot lost balance without leg actuation.

To further study the control system performance under off-road terrain conditions, we created and simulated the bikebot on the rugged terrain in simulation. The height of the terrain topography varies as a function of the xy coordinate as  $h=|0.07\sin(7x)-0.07\cos(4y+2)|$  m. Fig. 5(a) shows the xy view of the terrain surface and the height of the middle area

changes. The figure includes the bikebot trajectory and the foot contact points. We also include the EIC-based control without leg actuation as comparison. Figs. 5(b)-5(f) show the bikebot velocity v, roll angle  $\varphi_b$ , steering angle  $\phi$ , legground balance torque  $\tau_{q_x}$  and force  $f_x$ , respectively. When the bikebot moved on the rugged terrain, both velocity v and roll angle  $\varphi_b$  showed large oscillations compared with these that were running on the flat terrain at beginning and ending portions of the trajectory. The rough terrain also caused uncertainties to the leg-ground interaction as the leg-ground balance torque and force in Figs. 5(e) and 5(f) became noisy compared with that in Figs. 4(e) and 4(f). With only the steering control, the bikebot lost balance after the steering angle reached to the limit 30 deg, see Fig. 5(d). These results confirm that with the leg assistive balance torque, the bikebot maintains a low-speed movement on off-road, bumpy terrains.

#### V. CONCLUSION

This paper proposed to use the leg-ground interaction to provide assistive torque to balance the bikebot at lowspeed or off-road terrain conditions. Two assistive legs were installed on a bikebot to formulate a wheel-leg actuation mechanism and it was critical to have the leg actuation

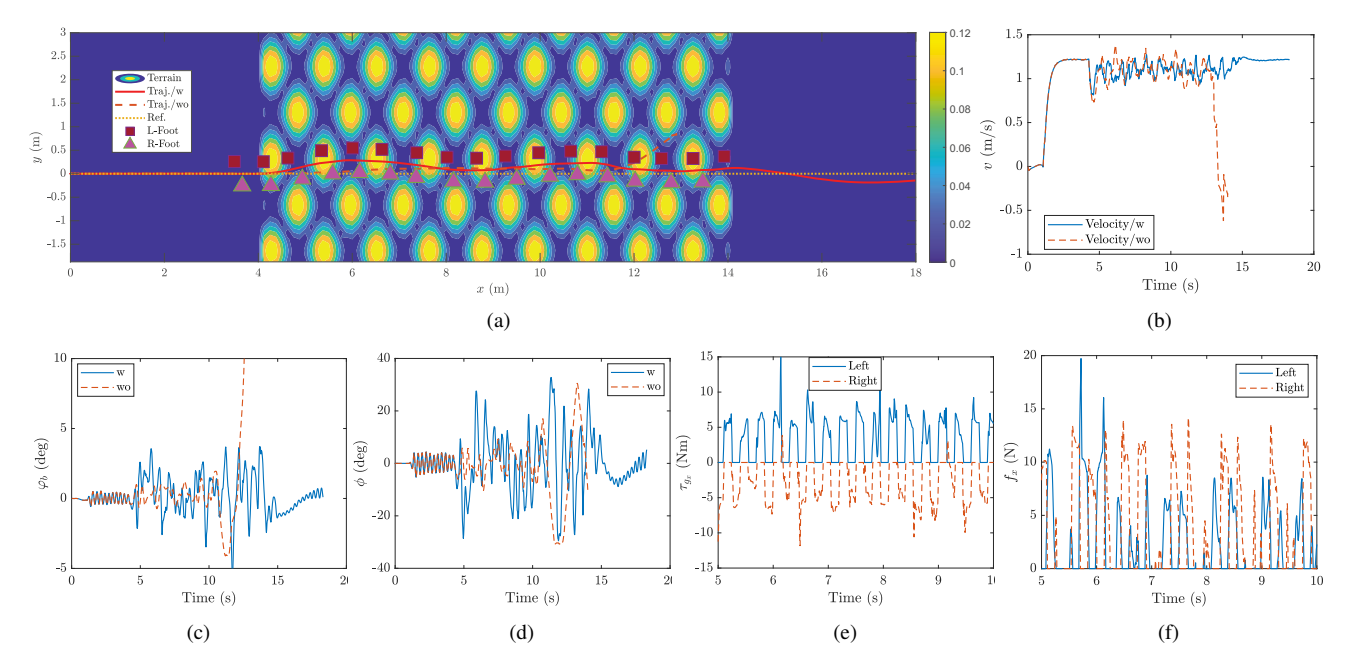


Fig. 5. Result for bikebot moving on a rugged area. (a) Bikebot trajectory with the leg footprint, (b) velocity, (c) roll angle, (d) steering angle, (e) leg-ground balance torque view of the robot schematics, and (f) leg-ground interaction force. The legends "w" and "wo" in (b) to (d) indicate the cases with and without using leg actuation, respectively.

when the steering-induced balance torque was limited. Based on the system dynamics, we formulated an MPC to design the leg-ground interaction force. The assistive leg actuation was integrated with the EIC-based navigation control design. We implemented and demonstrated the control design using a physics-engine based simulation package. The results showed that at low traveling velocity, the bikebot can follow a designed trajectory and keep balance on off-road, rugged terrains. We are currently implementing the proposed controller on the hardware system to conduct experiments and validate the design.

#### REFERENCES

- F. Han and J. Yi, "Stable learning-based tracking control of underactuated balance robots," *IEEE Robot. Automat. Lett.*, vol. 6, no. 2, pp. 1543–1550, 2021.
- [2] P. Wang, J. Yi, T. Liu, and Y. Zhang, "Trajectory tracking and balance control of an autonomous bikebot," in *Proc. IEEE Int. Conf. Robot. Autom.*, Singapore, 2017, pp. 2414–2419.
- [3] Y. Tanaka and T. Murakami, "Self sustaining bicycle robot with steering controller," in *Proc. 2004 IEEE Adv. Motion Contr. Conf.*, Kawasaki, Japan, 2004, pp. 193–197.
- [4] N. Getz, "Dynamic inversion of nonlinear maps with applications to nonlinear control and robotics," Ph.D. dissertation, Dept. Electr. Eng. and Comp. Sci., Univ. Calif., Berkeley, CA, 1995.
- [5] S. Lee and W. Ham, "Self-stabilzing strategy in tracking control of unmanned electric bicycle with mass balance," in *Proc. IEEE/RSJ Int. Conf. Intell. Robot. Syst.*, Lausanne, Switzerland, 2002, pp. 2200– 2205.
- [6] L. Cui, S. Wang, S. Yang, Z. Zhang, and Z.-P. Jiang, "Nonlinear balance control of an unmanned bicycle: Design and experiments," in *Proc. IEEE/RSJ Int. Conf. Intell. Robot. Syst.*, virtual conference, 2020, pp. 7279–7284.
- [7] L. Keo and M. Yamakita, "Control of an autonomous electric bicycle with both steering and balancer controls," *Adv. Robot.*, vol. 25, no. 1-2, pp. 1–22, 2011.
- [8] Y. Gong, K. Chen, J. Yi, and T. Liu, "Control of a two-wheel steering bikebot for agile maneuvers," in *Proc. IEEE/ASME Int. Conf. Adv. Intelli. Mechatronics*, Hong Kong, China, 2019, pp. 984–989.

- [9] Y. Zhang, J. Li, J. Yi, and D. Song, "Balance control and analysis of stationary riderless motorcycles," in *Proc. IEEE Int. Conf. Robot. Autom.*, Shanghai, China, 2011, pp. 3018–3023.
- [10] F. Han, A. Jelvani, J. Yi, and T. Liu, "Coordinated pose control of mobile manipulation with an unstable bikebot platform," *IEEE/ASME Trans. Mechatronics*, 2022, in press.
- [11] F. Han, X. Huang, Z. Wang, J. Yi, and T. Liu, "Autonomous bikebot control for crossing obstacles with assistive leg impulsive actuation," *IEEE/ASME Trans. Mechatronics*, 2022, in press.
- [12] Y. Zhang, P. Wang, J. Yi, D. Song, and T. Liu, "Stationary balance control of a bikebot," in *Proc. IEEE Int. Conf. Robot. Autom.*, Hong Kong, China, 2014, pp. 6706–6711.
- [13] P. Seekhao, K. Tungpimolrut, and M. Parnichkun, "Development and control of a bicycle robot based on steering and pendulum balancing," *Mechatronics*, vol. 69, pp. 1–12, 2020.
- [14] G. Valsecchi, R. Grandia, and M. Hutter, "Quadrupedal locomotion on uneven terrain with sensorized feet," *IEEE Robot. Automat. Lett.*, vol. 5, no. 2, pp. 1548–1555, 2020.
- [15] A. Shkolnik, M. Levashov, I. R. Manchester, and R. Tedrake, "Bounding on rough terrain with the LittleDog robot," *Int. J. Robot. Res.*, vol. 30, no. 2, pp. 192–215, 2011.
- [16] P. D. Neuhaus, J. E. Pratt, and M. J. Johnson, "Comprehensive summary of the institute for human and machine cognition's experience with littledog," *Int. J. Robot. Res.*, vol. 30, no. 2, pp. 216–235, 2011.
- [17] Y.-S. Kim, G.-P. Jung, H. Kim, K.-J. Cho, and C.-N. Chu, "Wheel transformer: A wheel-leg hybrid robot with passive transformable wheels," *IEEE Trans. Robotics*, vol. 30, no. 6, pp. 1487–1498, 2014.
- [18] P. Wang, J. Yi, and T. Liu, "Stability and control of a rider-bicycle system: Analysis and experiments," *IEEE Trans. Automat. Sci. Eng.*, vol. 17, no. 1, pp. 348–360, 2020.
- [19] H. J. Ferreau, C. Kirches, A. Potschka, H. G. Bock, and M. Diehl, "qpoases: A parametric active-set algorithm for quadratic programming," *Mathematical Programming Computation*, vol. 6, no. 4, pp. 327–363, 2014.
- [20] J. Di Carlo, P. M. Wensing, B. Katz, G. Bledt, and S. Kim, "Dynamic locomotion in the MIT cheetah 3 through convex model-predictive control," in *Proc. IEEE/RSJ Int. Conf. Intell. Robot. Syst.*, Madrid, Spain, 2018, pp. 7440–7447.
- [21] J. Hwangbo, J. Lee, and M. Hutter, "Per-contact iteration method for solving contact dynamics," *IEEE Robot. Automat. Lett.*, vol. 3, no. 2, pp. 895–902, 2018.